Chemical Science

EDGE ARTICLE

View Article Online
View Journal | View Issue

Cite this: *Chem. Sci.*, 2019, **10**, 829

All publication charges for this article have been paid for by the Royal Society of Chemistry

Crystallographic characterization of Lu_2C_{2n} ($2n$ = 76–90): cluster selection by cage size†

Wangqiang Shen,[a] Lipiao Bao,[a] Shuaifeng Hu,[a] Le Yang,[b] Peng Jin,*[b] Yunpeng Xie,*[a] Takeshi Akasaka[a] and Xing Lu*[a]

Received 31st August 2018
Accepted 27th October 2018

DOI: 10.1039/c8sc03886d

rsc.li/chemical-science

The successful isolation and unambiguous crystallographic assignment of a series of lutetium-containing endohedral metallofullerenes (EMFs), Lu_2C_{2n} ($2n$ = 76, 78, 80, 84, 86, 88, 90), reveal an unrecognized decisive effect of the cage size on the configuration of the encapsulated clusters. The molecular structures of these compounds are unambiguously assigned as $Lu_2@T_d(2)$-C_{76}, $Lu_2@D_{3h}(5)$-C_{78}, $Lu_2@C_{2v}(5)$-C_{80}, $Lu_2@C_{2v}(7)$-C_{84}, $Lu_2@C_s(8)$-C_{86}, $Lu_2@C_s(15)$-C_{86}, $Lu_2@C_1(26)$-C_{88}, $Lu_2C_2@C_{2v}(9)$-C_{86}, $Lu_2C_2@C_s(32)$-C_{88} and $Lu_2C_2@D_2(35)$-C_{88}. Specifically, when the cage is relatively small, $Lu_2@C_{2n}$ ($2n$ = 76–86) are all dimetallofullerenes (di-EMFs) and a Lu–Lu single bond could be formed between the two lutetium ions inside the cages. However, when the cage expands further, the valence electrons forming the possible Lu–Lu bond donate to a readily inserted C_2-unit, resulting in the formation of carbide EMFs, $Lu_2C_2@C_{2n}$ ($2n$ = 86, 88). Consistently, our theoretical results reveal that all these EMFs are thermodynamically favorable isomers. Thus the comprehensive characterization of the series of Lu_2C_{76-90} isomers and the overall agreement between the experimental and theoretical results reveal for the first time that the exact configuration of the internal metallic cluster is determined by the cage size, taking a solid step towards the controlled synthesis of novel hybrid molecules which may have potential applications as building blocks of single molecule devices.

Introduction

Putting metal atoms or metallic clusters into fullerenes has generated a new class of novel hybrid molecules, defined as endohedral metallofullerenes (EMFs), possessing novel structures and fascinating properties which are different from those of empty fullerenes.[1–4] During the last three decades, EMFs containing different metallic clusters, including metal nitride (M_3N),[5,6] metal carbide ($M_2C_2/M_3C_2/M_4C_2$),[7–9] metal sulfide (M_2S),[10,11] metal oxide ($M_2O/M_4O_2/M_4O_3$)[12–14] and metal cyanide (M_3CN/MCN)[15–17] clusters, have been structurally characterized in addition to the conventional EMFs containing only metal atoms ($M/M_2/M_3$).[18–20]

EMFs exhibit a variety of electronic and physicochemical properties which markedly depend on the nature of the encapsulated species.[21,22] One of the most brilliant features of EMFs is the charge transfer from the internal metallic species to the surrounding cage which is revealed to play an important role in determining the stability of the formed molecules.[2,3,23] For example, the $C_{2v}(9)$-C_{82} cage is the most stable one after accepting three electrons, and the corresponding $M@C_{2v}(9)$-C_{82} isomers have the highest production yield among all reported mono-EMFs for a variety of lanthanide elements regardless of the metal type.[24,25] As for cluster EMFs, theoretical and experimental results have suggested that the hexa-anionic $I_h(7)$-C_{80} cage is the most suitable candidate for encapsulating an M_3N (M = Sc, Y, Gd, Lu, *etc.*) cluster.[26,27]

In addition to the electronic interactions, the geometry of the cluster, especially the cluster size, also has a significant effect on the cage structure and symmetry. For instance, Dunsch and co-workers proposed theoretically that the small Sc_3N cluster presents a planar geometry inside the $D_{3h}(5)$-C_{78} cage, whereas the larger M_3N (M = Y, Lu, Dy, Tm) clusters prefer the $C_2(22\,010)$-C_{78} cage that violates the isolated pentagon rule (IPR) to keep their planarity.[28] And a subsequent experimental report confirmed that the large Gd_3N unit prefers to adopt the planar geometry in the $C_2(22\,010)$-C_{78} cage.[29] Another example demonstrated that M_3N clusters containing metals with a relatively small radius (*e.g.* Sc, Y and Gd) are preferentially encapsulated inside a C_{80} cage. In comparison, larger metals like La and Nd prefer to template C_{88} or C_{96}.[30,31] Accordingly, it seems that the size, shape, and charge of the encapsulated cluster play important roles in the selection of the complementary carbon cages. However, there is still a lack of experimental evidence to

[a]*State Key Laboratory of Materials Processing and Die & Mould Technology, School of Materials Science and Engineering, Huazhong University of Science and Technology, 1037 Luoyu Road, Wuhan, 430074, China. E-mail: lux@hust.edu.cn*

[b]*School of Materials Science and Engineering, Hebei University of Technology, Tianjin, 300130, China. E-mail: china.peng.jin@gmail.com*

† Electronic supplementary information (ESI) available. CCDC 1582214–1582219; 1836827–1836830. For ESI and crystallographic data in CIF or other electronic format see DOI: 10.1039/c8sc03886d

confirm whether the cage size has any influence on the cluster configuration or not. For example, Dunsch *et al.* proposed that the number of Sc atoms in the internal $Gd_xSc_{3-x}N$ clusters decreases along with the cage expansion (C_{78} to C_{88}), as demonstrated by absorption and vibrational spectroscopy, electrochemical studies and density functional theory (DFT) computations.[32] Popov *et al.* reported a systematic computational study on the analysis of the distortions in three classes of EMFs with nitride, sulfide, and carbide clusters, indicating that the preferable shapes of the internal clusters can be altered by the cage size.[33] Moreover, an interesting report from Dorn and co-workers theoretically revealed that the fullerene cage may compress the internal Y_2C_2 cluster to adopt different shapes, from butterfly-like configurations in small cages to nearly linear structures in large cages.[34] Nonetheless, there are no crystallographic results showing that the composition of the metallic species is controllable by the cage size.

We herein confirm for the first time that the exact form of the internal metallic cluster is determined by the cage size based on the concrete single-crystal X-ray crystallographic results of ten lutetium-containing endohedrals, namely, $Lu_2@T_d(2)$-C_{76}, $Lu_2@D_{3h}(5)$-C_{78}, $Lu_2@C_{2v}(5)$-C_{80}, $Lu_2@C_{2v}(7)$-C_{84}, $Lu_2@C_s(8)$-C_{86}, $Lu_2@C_s(15)$-C_{86}, $Lu_2@C_1(26)$-C_{88}, $Lu_2C_2@C_{2v}(9)$-C_{86}, $Lu_2C_2@C_s(32)$-C_{88} and $Lu_2C_2@D_2(35)$-C_{88}. It is revealed that the Lu–Lu distance increases along with the cage expansion as a direct result of the preferential coordination of the Lu atoms with the cage carbon atoms. Accordingly, the small cages can only accommodate a Lu_2 cluster because of the limited inner space, accompanied by the possible formation of a Lu–Lu bond. However, when the cage expands further, a C_2-unit is inserted between the two Lu atoms, which takes over partially the charges from the metals and coordinates with them, making the whole system more stable. The systematic characterization of Lu_2C_{76-90} isomers and the overall agreement between experimental and theoretical studies present concrete evidence for the decisive effect of the cage size on the composition of the encapsulated clusters of EMFs.

Results and discussion

Lu-EMFs were synthesized by a direct-current arc discharge method and pure isomers of Lu_2C_{2n} ($2n$ = 76, 78, 80, 84, 86, 88, 90) were obtained by multistage HPLC separation (see ESI, Fig. S1–S4 for details†). The analytical HPLC chromatograms (Fig. S5†) and the laser-desorption/ionization time-of-flight (LDI-TOF) mass spectra (Fig. S6†) of Lu_2C_{2n} ($2n$ = 76, 78, 80, 84, 86, 88, 90) isomers confirm their high purity. Fig. S7 and Table S1† show the visible-near-infrared (Vis-NIR) absorption spectra and the detailed characteristic bands of Lu_2C_{76-90} isomers dissolved in carbon disulfide (CS_2), respectively. The absorption spectra of $Lu_2@C_{2v}(7)$-C_{84}, $Lu_2@C_s(8)$-C_{86}, $Lu_2@C_s(15)$-C_{86}, $Lu_2@C_1(26)$-C_{88} and $Lu_2C_2@C_s(32)$-C_{88} are quite different from those of the corresponding EMFs possessing C_{84}, C_{86} and C_{88} cages reported before,[15,35–43] indicating their different structures.

Finally, the molecular structures of Lu_2C_{2n} ($2n$ = 76, 78, 80, 84, 86, 88, 90) isomers were unambiguously determined by single-crystal X-ray diffraction (XRD) crystallography to be $Lu_2@T_d(2)$-C_{76}, $Lu_2@D_{3h}(5)$-C_{78}, $Lu_2@C_{2v}(5)$-C_{80}, $Lu_2@C_{2v}(7)$-C_{84}, $Lu_2@C_s(8)$-C_{86}, $Lu_2@C_s(15)$-C_{86}, $Lu_2@C_1(26)$-C_{88}, $Lu_2C_2@C_{2v}(9)$-C_{86}, $Lu_2C_2@C_s(32)$-C_{88} and $Lu_2C_2@D_2(35)$-C_{88}, respectively, taking advantage of the high-quality of the co-crystals of Lu_2C_{2n}/Ni^{II}(OEP) (OEP = 2,3,7,8,12,13,17,18-octaethylporphyrin dianion). Although $Lu_2@T_d(2)$-C_{76} was first isolated and confirmed to have a T_d-symmetric cage according to ^{13}C NMR spectroscopic studies in combination with scanning tunneling microscopy results,[44] and $D_{3h}(5)$-C_{78}, $C_{2v}(5)$-C_{80}, $C_{2v}(9)$-C_{86} and $D_2(35)$-C_{88} cages were obtained and crystallographically characterized for EMFs possessing the same cage symmetry, such as $Sc_2O@D_{3h}(5)$-C_{78},[45] $Sc_2O@C_{2v}(5)$-C_{80},[12] $Sc_2C_2@C_{2v}(9)$-C_{86} (ref. 36) and $Sm_2@D_2(35)$-C_{88},[40] it is noteworthy that the cages of $C_{2v}(7)$-C_{84}, $C_s(8)$-C_{86}, $C_s(15)$-C_{86}, $C_1(26)$-C_{88} and $C_s(32)$-C_{88} have never been experimentally reported before in spite of the fact that $Sc_2O@C_{2v}(7)$-C_{84} was theoretically predicted without further experimental evidence.[46]

Fig. 1 and 2 portray the molecular structures of $Lu_2@C_{2n}$ ($2n$ = 76, 78, 80, 84, 86, 88, 90) isomers co-crystallized with the Ni^{II}(OEP) molecules. For $Lu_2@C_s(8)$-C_{86} and $Lu_2C_2@D_2(35)$-C_{88}, each fullerene cage is surrounded by two Ni^{II}(OEP) molecules in a sandwich-like arrangement, and the ethyl groups of one of the Ni^{II}(OEP) molecules are arranged in such a way that they can embrace the fullerene cage from both sides whereas the other endohedrals adopt the normal one-EMF-one-Ni(OEP) fashion. The shortest Ni-cage distances in all the systems fall in the range of 2.631 Å–3.050 Å, suggesting substantial π–π interactions between the fullerene cage and the Ni^{II}(OEP) molecule(s).[47–49] Inside these cages, the Lu atoms show severe disorder in all EMFs (Fig. 3, Tables S2 and S3, ESI†), indicating a motional behavior of the two Lu ions which may account for the strong Lu-cage interactions by fulfilling the coordination requirements of the Lu ions as much as possible. In detail, 19, 16 and 27 Lu positions are found for the two Lu atoms inside the $Lu_2@T_d(2)$-C_{76}, $Lu_2@D_{3h}(5)$-C_{78} and $Lu_2@C_{2v}(5)$-C_{80} cages, respectively, whereas 26, 13 and 20 Lu sites are positioned for the two Lu atoms in the respective $Lu_2@C_{2v}(7)$-C_{84}, $Lu_2@C_s(8)$-C_{86}, $Lu_2@C_s(15)$-C_{86} cage. In $Lu_2@C_1(26)$-C_{88}, 27 Lu sites are positioned for the two Lu atoms. Moreover, 13, 24 and 16 Lu sites are found for the two Lu atoms in $Lu_2C_2@C_{2v}(9)$-C_{86}, $Lu_2C_2@C_s(32)$-C_{88} and $Lu_2C_2@D_2(35)$-C_{88}, respectively.

Furthermore, the representative structural data of $Lu_2@C_{76-90}$ isomers, such as the cage length/width ratio (L/W ratio), major Lu–Lu distance, Lu–Lu distance range and Lu-cage distance, are summarized in Table 1. The Lu–Lu distances between any two opposite Lu sites with comparable occupancy values are in the range of 3.31–3.53 Å, 3.27–3.67 Å, 3.22–3.73 Å, 3.33–3.84 Å, 3.49–3.73 Å, 3.34–3.84 Å and 3.57–3.62 Å for $Lu_2@T_d(2)$-C_{76}, $Lu_2@D_{3h}(5)$-C_{78}, $Lu_2@C_{2v}(5)$-C_{80}, $Lu_2@C_{2v}(7)$-C_{84}, $Lu_2@C_s(8)$-C_{86}, $Lu_2@C_s(15)$-C_{86} and $Lu_2@C_1(26)$-C_{88}, respectively. In contrast, for $Lu_2C_2@C_{2v}(9)$-C_{86}, $Lu_2C_2@C_s(32)$-C_{88} and $Lu_2C_2@D_2(35)$-C_{88}, which possess relatively large cages, the respective Lu–Lu distances are much longer and fall in 3.94–4.43 Å, 4.45–4.66 Å and 4.14–4.41 Å, respectively. Therefore, in these cages, a C_2-unit is inserted between the two Lu atoms, which fulfills the coordination

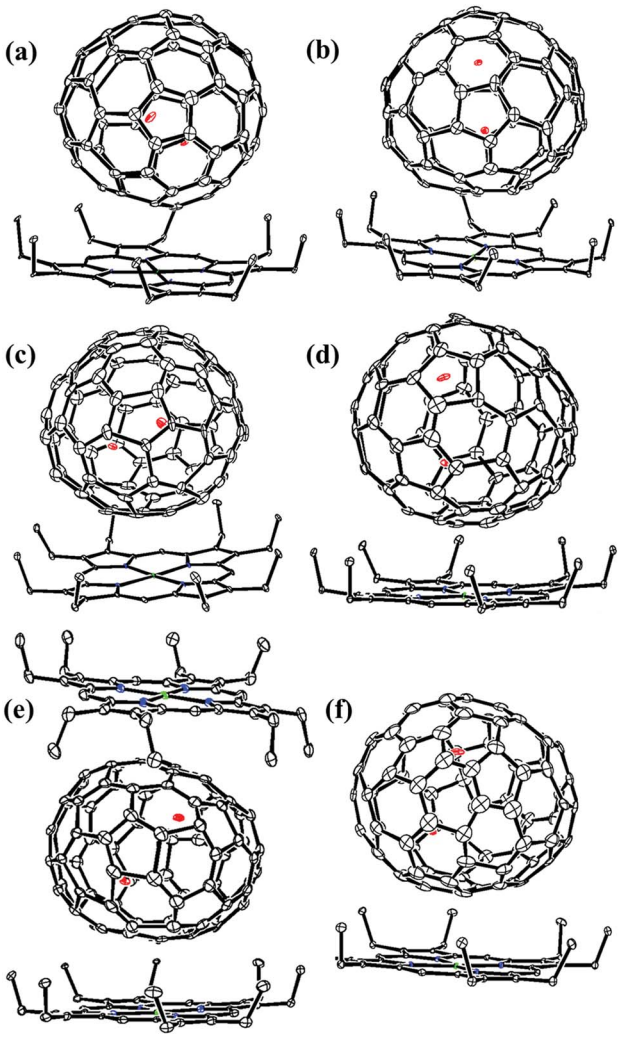

Fig. 1 ORTEP drawings of (a) $Lu_2@T_d(2)$-C_{76}·Ni^{II}(OEP), (b) $Lu_2@D_{3h}(5)$-C_{78}·Ni^{II}(OEP), (c) $Lu_2@C_{2v}(5)$-C_{80}·Ni^{II}(OEP), (d) $Lu_2@C_{2v}(7)$-C_{84}-·Ni^{II}(OEP), (e) $Lu_2@C_s(8)$-C_{86}·1.5Ni^{II}(OEP) and (f) $Lu_2@C_s(15)$-C_{86}-·Ni^{II}(OEP). Thermal contours are drawn at the 10% probability level. Only one fullerene cage and the predominant metal sites are shown, whereas minor metal sites, solvent molecules and H atoms are omitted for clarity.

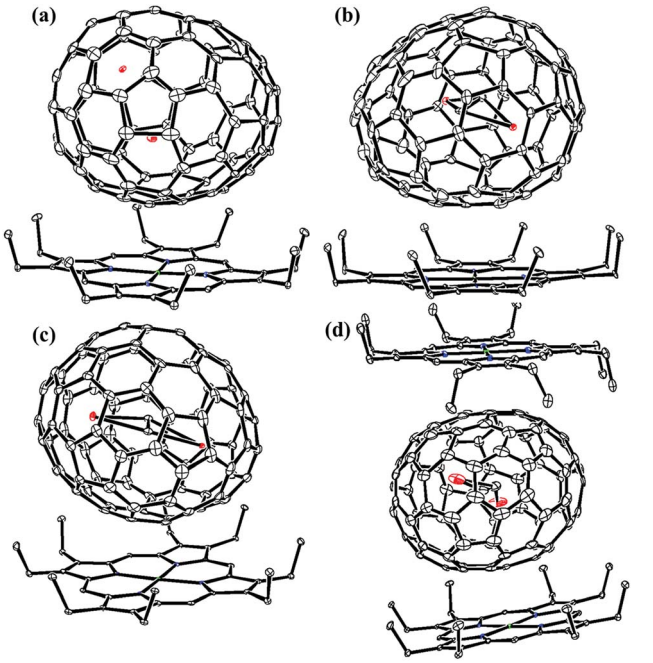

Fig. 2 ORTEP drawings of (a) $Lu_2@C_1(26)$-C_{88}·Ni^{II}(OEP), (b) $Lu_2C_2@C_{2v}(9)$-C_{86}·Ni^{II}(OEP), (c) $Lu_2C_2@C_s(32)$-C_{88}·Ni^{II}(OEP) and (d) $Lu_2C_2@D_2(35)$-C_{88}·Ni^{II}(OEP). Thermal contours are drawn at the 10% probability level. Only one fullerene cage and the predominant metal sites are shown, whereas minor metal sites, solvent molecules and H atoms are omitted for clarity.

requirement of the Lu ions by taking over partially the charges from the metal ions. The shortest Lu-cage distances are consistently 2.108 Å, 2.263 Å, 2.065 Å, 2.106 Å, 2.086 Å, 2.103 Å, 2.291 Å, 2.269 Å, 2.319 Å and 2.166 Å for $Lu_2@T_d(2)$-C_{76}, $Lu_2@D_{3h}(5)$-C_{78}, $Lu_2@C_{2v}(5)$-C_{80}, $Lu_2@C_{2v}(7)$-C_{84}, $Lu_2@C_s(8)$-C_{86}, $Lu_2@C_s(15)$-C_{86}, $Lu_2@C_1(26)$-C_{88}, $Lu_2C_2@C_{2v}(9)$-C_{86}, $Lu_2C_2@C_s(32)$-C_{88} and $Lu_2C_2@D_2(35)$-C_{88}, respectively, which are all shorter than the calculated values for $Lu_2@T_d$-C_{76} (2.37–2.42 Å),[50,51] suggesting strong Lu-cage interactions.

It is interesting to find that the small cages (C_{76-86}) prefer to accommodate a Lu_2 dimer to form di-EMFs whereas carbide cluster metallofullerenes (CCMFs) are formed for Lu_2C_{88} or Lu_2C_{90}, which possess relatively large cages. We speculate that this phenomenon is caused by the different cage structure parameters, particularly the cage length and width. As clearly shown in Table 1, the cage length and L/W ratio increase in accordance with cage expansion, resulting in a substantial increase of the Lu–Lu distance. In particular, C_{86}-based lutetium-containing EMFs have two different compositions: $C_s(8)$-C_{86} (L/W ratio = 1.16) and $C_s(15)$-C_{86} (L/W ratio = 1.16) possess relatively round cages and they choose to encapsulate a Lu_2 dimer instead of a Lu_2C_2 cluster because of the limited inner space, whereas the elongated $C_{2v}(9)$-C_{86} (L/W ratio = 1.20) causes the increased Lu–Lu distance because of strong Lu-cage interactions and easy C_2 insertion, resulting in the formation of the CCMF $Lu_2C_2@C_{2v}(9)$-C_{86}. As a matter of fact, the cages smaller than C_{86} can only accommodate a Lu_2 dimer and the larger ones always prefer the Lu_2C_2 composition to make the resultant EMFs more stable.[49,52]

Fig. S8† shows the location of the major Lu_2/Lu_2C_2 cluster relative to the cage orientation in the ten EMFs under study. In $Lu_2@C_{2v}(5)$-C_{80}, $Lu_2@C_{2v}(7)$-C_{84}, $Lu_2@C_s(8)$-C_{86}, $Lu_2@C_1(26)$-C_{88} and $Lu_2C_2@C_s(32)$-C_{88}, one major Lu site is situated over a [5,6]-bond, whereas the other one is close to a hexagonal ring. In the other five endohedrals, each prominent Lu position is located over a [5,6]-bond. Moreover, the configurations of the Lu_2C_2 clusters inside the carbon cages are all shaped like a butterfly with two tightly bonded carbon atoms in the respective cage centers. The Lu–C–C–Lu dihedral angles are 132.13°, 145.46° and 142.83° in the $C_{2v}(9)$-C_{86}, $C_s(32)$-C_{88} and $D_2(35)$-C_{88} cages, respectively. Furthermore, the C–C bond lengths of the C_2 unit in $Lu_2C_2@C_{2v}(9)$-C_{86}, $Lu_2C_2@C_s(32)$-C_{88} and $Lu_2C_2@D_2(35)$-C_{88} are 1.11 Å, 1.20 Å and 1.00 Å, respectively, which represent typical C–C triple bonds (Fig. S8†).

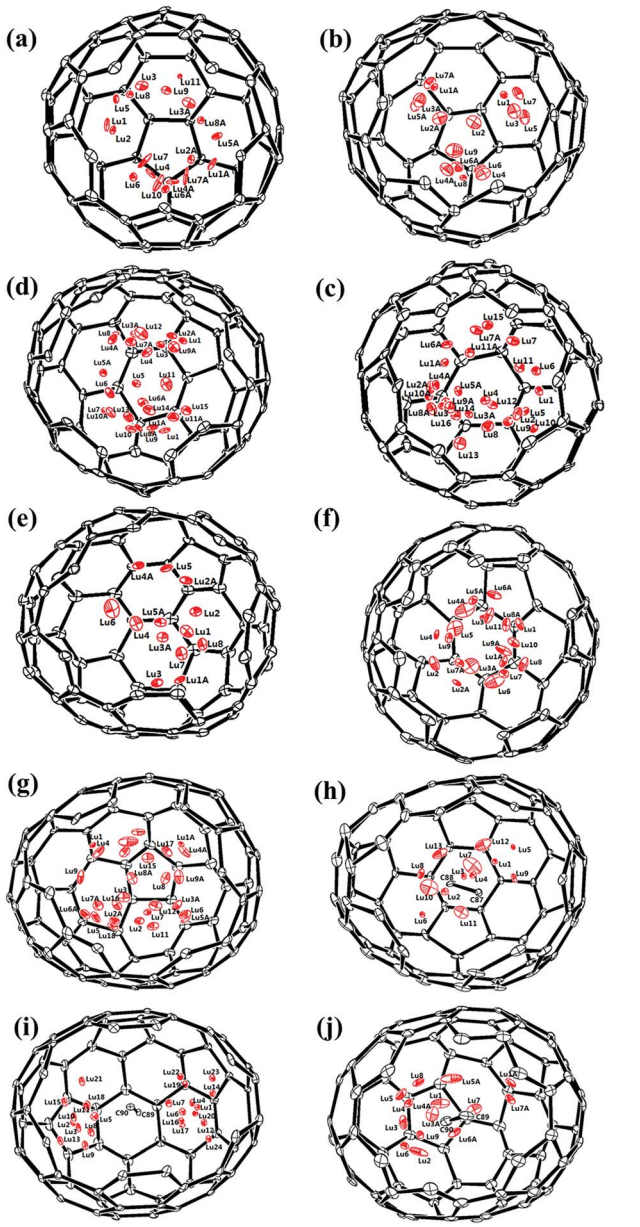

Fig. 3 Perspective drawings showing the disordered lutetium sites. (a) 19 in $Lu_2@T_d(2)$-C_{76}, (b) 16 in $Lu_2@D_{3h}(5)$-C_{78}, (c) 27 in $Lu_2@C_{2v}(5)$-C_{80}, (d) 26 in $Lu_2@C_{2v}(7)$-C_{84}, (e) 13 in $Lu_2@C_s(8)$-C_{86}, (f) 20 in $Lu_2@C_s(15)$-C_{86}, (g) 27 in $Lu_2@C_1(26)$-C_{88}, (h) 13 in $Lu_2C_2@C_{2v}(9)$-C_{86}, (i) 24 in $Lu_2C_2@C_s(32)$-C_{88} and (j) 16 in $Lu_2C_2@D_2(35)$-C_{88}.

The redox behaviors of the EMFs under study are characterized by cyclic voltammetry (CV) except for $Lu_2@D_{3h}(5)$-C_{78} and $Lu_2@C_{2v}(5)$-C_{80} due to their extremely low yields (Fig. S9 and S10†). In general, these compounds display one or two oxidation steps together with four reduction steps within the solvent window. It is noteworthy that the electrochemical gaps of Lu_2C_{2n} ($2n = 76$, 82, 84, 86, 88, 90) isomers are relatively large (1.19 eV–1.39 eV), indicating their high stability. Moreover, it appears that the CCMFs show better reversibility of the redox processes than the di-EMFs. For instance, several irreversible processes, either reduction or oxidation, are found for $Lu_2@T_d(2)$-C_{76}, $Lu_2@C_{2v}(7)$-C_{84}, $Lu_2@C_s(8)$-C_{86} and $Lu_2@C_1(26)$-C_{88}, but all of the two oxidation and the four reduction processes are reversible for $Lu_2C_2@C_s(32)$-C_{88} and $Lu_2C_2@D_2(35)$-C_{88}. Table S6† lists the electrochemical potentials of the EMFs under study. In particular, the first and the second reduction potentials are mutually very close, as are the third and the fourth, but the gap between the third and the second is generally large. These results strongly corroborate their closed-shell electronic configuration with nondegenerate low-lying LUMO and accessible LUMO+1 orbitals. Consequently, such electrochemical behaviors can be regarded as characteristic properties of Lu_2C_{2n}-type EMFs.[53] Accordingly, there are no EPR signals for all the EMFs reported here because of their closed-shell electronic configuration.

The unobserved decisive effect of the cage size on the configuration of the encapsulated clusters stimulates our interest to find a reasonable explanation. DFT calculations at the M06-2X/6-31G*∼SDD level were thus conducted to rationalize the formation of these Lu_2C_{2n} ($2n = 76$, 78, 80, 84, 86, 88, 90) isomers. Fig. 4 depicts their optimized geometries, which agree well with their respective X-ray structures. The lutetium element has a $[Xe]4f^{14}6s^25d^1$ electronic configuration and may keep its 6s electrons due to the relativistic contraction and large stabilization of the 6s atomic orbital. For $Lu_2@C_{76-88}$ isomers, the calculated Lu–Lu distances range from 3.41 Å to 3.72 Å, and are all comparable to those observed from our crystallographic data (Tables 1 and S7†). Actually, our results are perfectly consistent with the theoretical predictions reported by Popov and co-workers, who proposed that lutetium atoms are more inclined to adopt the +2 state, and accordingly, Lu–Lu bonding could be favorable in lutetium-containing EMFs.[54,55] In comparison, the calculated Lu–Lu distances in $Lu_2C_2@C_{2v}(9)$-C_{86}, $Lu_2C_2@C_s(32)$-C_{88} and $Lu_2C_2@D_2(35)$-C_{88} are as long as 4.37 Å, 4.64 Å and 4.64 Å, respectively, indicating the insertion of a C_2-unit.

Natural bond orbital (NBO) analysis demonstrates that the two Lu atoms in $Lu_2@C_{76-88}$ may form a Lu–Lu single bond with an electron occupancy of 1.97–1.98 e, which is supported by the calculated Wiberg bond orders (WBOs) ranging from 0.94 to 0.98 (Table S7†). Moreover, consistent with the low-lying $(6s)\sigma_g^2$ molecular orbital of the free Lu_2 dimer, the possible Lu–Lu bonds have an spd-hybrid character with the Lu-6s orbitals contributing the most to the metal bonding MOs, and each Lu atom donates one 5d electron and one 6s electron to the cage with the 4f electrons remaining intact. However, for $Lu_2C_2@C_{86-88}$, the Lu–Lu single bond could not be formed in the corresponding cage because the valence electrons are partially donated to the C_2-unit, as indicated by the calculated small WBO values ranging from 0.15 to 0.17 (Table S7†), resulting in the formation of the Lu_2C_2 units.

Furthermore, we optimized the structures of different Lu_2C_{2n} ($2n = 76$, 78, 80, 84, 86, 88, 90) isomers in either the $Lu_2@C_{2n}$ or $Lu_2C_2@C_{2n-2}$ form based on a series of low-energy C_{74-90}^{4-} cages to differentiate their relative stability. Fig. S11–S17† and Table 2 show the optimized structures of the low-energy Lu_2C_{76-90} isomers and relative energies as well as HOMO–LUMO gap energies. As clearly shown in Table 2, both $Lu_2@T_d(2)$-C_{76} and $Lu_2@D_{3h}(5)$-C_{78} are the lowest-energy ones among all the

Table 1 Cage size, length/width (L/W) ratio, major Lu-Lu distance, calculated Lu-Lu distance, Lu-Lu distance range and the shortest Lu-cage distance of $Lu_2@T_d(2)$-C_{76}, $Lu_2@D_{3h}(5)$-C_{78}, $Lu_2@C_{2v}(5)$-C_{80}, $Lu_2@C_s(6)$-C_{82},[39] $Lu_2@C_{3v}(8)$-C_{82},[39] $Lu_2@D_{2d}(23)$-C_{84},[39] $Lu_2@C_{2v}(7)$-C_{84}, $Lu_2@C_{2v}(9)$-C_{86},[39] $Lu_2@C_s(8)$-C_{86}, $Lu_2@C_s(15)$-C_{86}, $Lu_2@C_1(26)$-C_{88}, $Lu_2C_2@C_{2v}(9)$-C_{86}, $Lu_2C_2@C_s(32)$-C_{88} and $Lu_2C_2@D_2(35)$-C_{88}

Compound	Cage length (Å)	Cage width (Å)	L/W ratio	Major Lu–Lu distance (Å)[a]	Calculated Lu–Lu distance (Å)	Lu–Lu distance range (Å)[b]	Shortest Lu-cage distance[c]
$Lu_2@T_d(2)$-C_{76}	7.126	7.110	1.00	3.50	3.44	3.14–3.50	2.054
$Lu_2@D_{3h}(5)$-C_{78}	8.338	7.548	1.10	3.27	3.41	3.27–3.67	2.263
$Lu_2@C_{2v}(5)$-C_{80}	8.245	7.896	1.04	3.60	3.72	3.22–3.73	2.065
$Lu_2@C_{3v}(8)$-C_{82}	8.400	8.315	1.01	3.21	3.47	3.21–3.57	2.299
$Lu_2@C_s(6)$-C_{82}	8.413	7.739	1.08	3.59	3.60	3.35–3.67	2.243
$Lu_2@D_{2d}(23)$-C_{84}	8.212	7.934	1.04	3.75	4.00	3.24–3.75	2.135
$Lu_2@C_{2v}(7)$-C_{84}	8.502	8.199	1.04	3.56	3.46	3.33–3.84	2.106
$Lu_2@C_{2v}(9)$-C_{86}	8.991	7.553	1.09	3.43	3.70	3.43–3.72	2.293
$Lu_2@C_s(8)$-C_{86}	8.455	7.296	1.16	3.49	3.53	3.49–3.73	2.086
$Lu_2@C_s(15)$-C_{86}	8.611	7.454	1.16	3.34	3.67	3.34–3.84	2.103
$Lu_2@C_1(26)$-C_{88}	9.018	7.501	1.20	3.57	3.65	3.57–3.62	2.291
$Lu_2C_2@C_{2v}(9)$-C_{86}	8.986	7.502	1.18	4.41	4.37	3.94–4.43	2.269
$Lu_2C_2@C_s(32)$-C_{88}	8.883	7.124	1.25	4.66	4.64	4.45–4.66	2.319
$Lu_2C_2@D_2(35)$-C_{88}	9.104	7.184	1.27	4.41	4.64	4.14–4.41	2.166

[a] Lu–Lu distance between the major Lu sites. [b] Lu–Lu distance between any two opposite Lu sites with comparable occupancy. [c] The shortest Lu-cage distance between the major Lu sites and the cage carbon atoms.

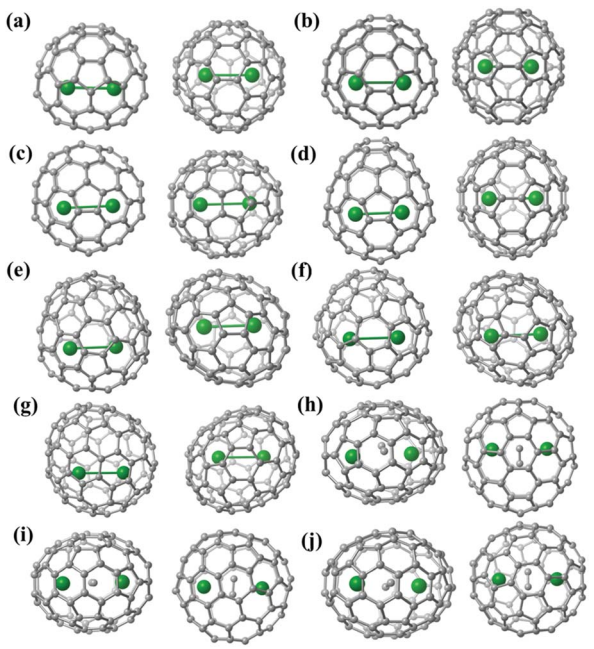

Fig. 4 Optimized structures of (a) $Lu_2@T_d(2)$-C_{76}, (b) $Lu_2@D_{3h}(5)$-C_{78}, (c) $Lu_2@C_{2v}(5)$-C_{80}, (d) $Lu_2@C_{2v}(7)$-C_{84}, (e) $Lu_2@C_s(8)$-C_{86}, (f) $Lu_2@C_s(15)$-C_{86}, (g) $Lu_2@C_1(26)$-C_{88}, (h) $Lu_2C_2@C_{2v}(9)$-C_{86}, (i) $Lu_2C_2@C_s(32)$-C_{88} and (j) $Lu_2C_2@D_2(35)$-C_{88} (top and side views).

considered isomers. Moreover, $Lu_2@I_h(7)$-C_{80} is 6.6 kcal mol^{-1} lower in energy than $Lu_2@C_{2v}(5)$-C_{80} when it has a triplet ground state. Therefore, it is highly possible that $Lu_2@I_h(7)$-C_{80} is generated together with $Lu_2@C_{2v}(5)$-C_{80} during the arc-discharge process, but it may form insoluble products in the raw soot due to its radical character and thus is absent in the usual solvent extract (Table 2).[56–58] As for Lu_2C_{82}, a previous report has revealed that $Lu_2@C_s(6)$-C_{82} and $Lu_2@C_{3v}(8)$-C_{82} are both lower in energy than any of the $Lu_2C_2@C_{80}$ isomers (Table 2).[39] Accordingly, for a composition of Lu_2C_{76-82}, $Lu_2@C_{2n}$ is always more stable than the corresponding carbide form $Lu_2C_2@C_{2n-2}$, indicating that the formation of di-EMFs is energetically favorable within this cage size range.

However, Lu_2C_{84-86}, $Lu_2@C_{2v}(7)$-C_{84}, $Lu_2@C_s(8)$-C_{86}, and $Lu_2@C_s(15)$-C_{86} and their respective $Lu_2C_2@C_{2n-2}$ isomers are mixed in energy, with the recently reported $Lu_2@D_{2d}(23)$-C_{84} and $Lu_2@C_{2v}(9)$-C_{86} being the most stable ones (Table 2).[39] These results imply that the formation of CCMFs is gradually favored with increasing cage size. Indeed, as shown in Fig. S16 and S17,† $Lu_2C_2@C_{2v}(9)$-C_{86}, $Lu_2C_2@D_2(35)$-C_{88} and $Lu_2C_2@C_s(32)$-C_{88} are the lowest-energy Lu_2C_{88} and Lu_2C_{90} isomers, respectively. Therefore, as the cage size increases to C_{88} and C_{90}, the CCMFs are energetically more stable than the corresponding di-EMFs.

Overall, our experimental and theoretical results have unambiguously confirmed that the exact composition of the internal cluster is changed from Lu_2 to Lu_2C_2 along with the cage expansion, which is a synergetic result of C2 insertion and the strong Lu-cage coordination of the Lu ions with the cage carbon atoms. It appears that the C_{86} cage is a threshold for Lu_2C_{2n}-type EMFs transforming from di-EMFs to CCMFs. If the transformation is a common phenomenon in other systems, it is expected that larger metals such as erbium, gallium and lanthanum may prefer a larger cage for the transformation from M_2 to M_2C_2 (M = Er, Gd, La). Indeed, Balch. *et al.* have separated two Gd_2C_{94} isomers, one of which is structurally confirmed to be a CCMF, namely $Gd_2C_2@D_3(85)$-C_{92}, while the other is theoretically proposed to be a conventional endohedral, $Gd_2@C_2(121)$-C_{94}.[59] A more recent study reported the isolation and crystallographic elucidation of an Er-based CCMF, *i.e.* $Er_2C_2@D_3(85)$-C_{92}, confirming again that larger cages tend to accommodate the carbide cluster.[60] Moreover, for the even larger La^{3+} ions, although the structures of some di-EMFs,

Table 2 Optimized structures of low-lying Lu_2C_{76-90} isomers with relative energies (kcal mol^{-1}) and HOMO–LUMO gap energies (eV, in parentheses). The isomers labeled in bold are experimentally observed

Compounds	Relative energies of the selected low-lying isomers				
Lu_2C_{76}	**Lu_2@T_d(2)-C_{76}, 0.0 (2.95)**	Lu_2C_2@C_2(13333)-C_{74}, 9.9 (2.98)	Lu_2C_2@C_1(13334)-C_{74}, 17.3 (3.08)	Lu_2@C_{2v}(19138)-C_{76}, 19.5 (1.75)	Lu_2C_2@C_1(13384)-C_{74}, 22.7 (3.03)
Lu_2C_{78}	**Lu_2@D_{3d}(5)-C_{78}, 0.0 (2.41)**	Lu_2@C_{2v}(3)-C_{78}, 5.2 (2.96)	Lu_2@C_s(24099)-C_{78}, 12.7 (2.74)	Lu_2@C_1(22595)-C_{78}, 13.1 (2.89)	Lu_2C_2@T_d(2)-C_{76}, 16.4 (2.81)
Lu_2C_{80}	Lu_2@I_h(7)-C_{80}, 0.0 (3.31/2.03)	**Lu_2@C_{2v}(5)-C_{80}, 6.6 (2.88)**	Lu_2@D_{5h}(6)-C_{80}, 8.0 (2.26)	Lu_2@C_1(31 891)-C_{80}, 26.4 (2.51)	Lu_2C_2@D_{3d}(5)-C_{78}, 30.0 (2.60)
Lu_2C_{82}	**Lu_2@C_{3v}(8)-C_{82},[39] 0.0 (3.39)**	**Lu_2@C_s(6)-C_{82},[39] 0.5 (3.03)**	Lu_2C_2@C_{2v}(5)-C_{80}, 19.7 (2.94)	Lu_2C_2@D_{5h}(6)-C_{80}, 22.7 (2.37)	Lu_2C_2@I_h(7)-C_{80}, 31.5 (2.16)
Lu_2C_{84}	**Lu_2@D_{2d}(23)-C_{84},[39] 0.0 (2.99)**	Lu_2C_2@C_{3v}(8)-C_{82}, 6.2 (3.42)	**Lu_2@C_{2v}(7)-C_{84}, 6.4 (3.19)**	Lu_2C_2@C_s(6)-C_{82}, 6.6 (3.08)	Lu_2C_2@C_{2v}(9)-C_{82}, 8.7 (2.62)
Lu_2C_{86}	**Lu_2@C_{2v}(9)-C_{86},[39] 0.0 (3.10)**	Lu_2C_2@D_{2d}(23)-C_{84}, 8.9 (3.02)	**Lu_2@C_s(8)-C_{86}, 9.9 (3.37)**	Lu_2C_2@C_1(51383)-C_{84}, 13.2 (3.04)	**Lu_2@C_s(15)-C_{86}, 15.6 (2.77)**
Lu_2C_{88}	**Lu_2C_2@C_{2v}(9)-C_{86}, 0.0 (3.02)**	**Lu_2@C_1(26)-C_{88}, 2.9 (3.06)**	Lu_2C_2@C_1(13)-C_{86}, 13.5 (2.91)	Lu_2@C_1(30)-C_{88}, 14.4 (2.64)	Lu_2C_2@C_s(15)-C_{86}, 14.4 (2.62)
Lu_2C_{90}	**Lu_2C_2@D_2(35)-C_{88}, 0.0 (2.86)**	**Lu_2C_2@C_s(32)-C_{88}, 1.5 (2.85)**	Lu_2@D_{5h}(41)-C_{90}, 5.6 (2.73)	Lu_2@C_1(43)-C_{90}, 6.5 (2.60)	Lu_2@C_1(21)-C_{90}, 8.5 (3.00)

namely La_2@D_2(10611)-C_{72},[61] La_2@C_s(17490)-C_{76},[62] La_2@D_{3h}(5)-C_{78},[63] La_2@I_h(7)-C_{80},[64] and La_2@D_5(450)-C_{100} [65] have been confirmed by single crystal XRD crystallography, the La^{3+} ions are also more inclined to form carbide structures with some giant cages such as C_{90-104}, which are rationalized by considering the synergistic effect of inserting a C_2-unit on the stabilization of CCMFs both electronically and geometrically.[47–49]

Conclusions

In summary, a series of lutetium-containing EMFs, namely Lu_2@T_d(2)-C_{76}, Lu_2@D_{3h}(5)-C_{78}, Lu_2@C_{2v}(5)-C_{80}, Lu_2@C_{2v}(7)-C_{84}, Lu_2@C_s(8)-C_{86}, Lu_2@C_s(15)-C_{86}, Lu_2@C_1(26)-C_{88}, Lu_2C_2@C_{2v}(9)-C_{86}, Lu_2C_2@C_s(32)-C_{88} and Lu_2C_2@D_2(35)-C_{88}, have been isolated and structurally determined. Based on our experimental and theoretical results, a clear correlation between the cage size and the configuration of the internal metallic cluster is revealed. Moreover, we also propose that the C_{86} cage is the threshold for Lu_2C_{2n}-type EMFs transforming from di-EMFs to CCMFs. Specifically, the relatively small cages, *i.e.* C_{76-86}, choose to encapsulate a Lu_2 cluster with the possible formation of a Lu–Lu bond because of the limited inner space. However, further cage expansion elongates the Lu–Lu distance due to the strong Lu-cage interactions and the insertion of a C_2-unit, resulting in the formation of CCMFs, Lu_2C_2@C_{2n} ($2n = 86$, 88). Accordingly, we confirm for the first time that the preferential formation of the Lu_2@C_{2n}/Lu_2C_2@C_{2n-2} composition is determined by the cage size, presenting a practical strategy for the templated synthesis of EMFs possessing desired internal clusters, which may facilitate the application of EMFs as building blocks for molecular devices/machines.

Experimental

Synthesis and isolation of Lu_2C_{2n} ($2n = 76$, 78, 80, 84, 86, 88, 90)

Soot containing Lu-EMFs was synthesized by a direct-current arc discharge method and was extracted using carbon disulfide (CS_2). After the removal of CS_2, the residue was dissolved in toluene and the solution was subjected to a multi-stage high-performance liquid chromatography (HPLC) separation. The experimental details are given in the ESI.†

General characterization

High-performance liquid chromatography (HPLC) was conducted on an LC-9130 NEXT machine (Japan Analytical Industry Co., Ltd.) with toluene as the mobile phase. Matrix-assisted laser desorption/ionization time-of-flight (MALDI-TOF) mass spectrometry was performed on a BIFLEX III spectrometer (Bruker Daltonics Inc., Germany). Vis-NIR spectra were obtained on a PE Lambda 750S spectrophotometer in CS_2. Cyclic voltammograms (CV) were measured in 1,2-dichlorobenzene with 0.05 M *n*-Bu_4NPF_6 as the supporting electrolyte at a Pt working electrode with a CHI660E workstation.

Single crystal XRD measurements of Lu_2C_{2n} ($2n$ = 76, 78, 80, 84, 86, 88, 90)

The crystallographic data are shown in Tables S4 and S5.† Crystalline blocks of Lu_2C_{2n} ($2n$ = 76, 78, 80, 84, 86, 88, 90) isomers were obtained by layering a benzene solution of Ni^{II}(OEP) over a CS_2 solution of the corresponding metallofullerenes at room temperature. Over a 20-day period, the two solutions diffused together, and black crystals formed. Single-crystal XRD measurement of $Lu_2@C_s(8)$-C_{86}, $Lu_2@C_s(15)$-C_{86} and $Lu_2C_2@C_{2v}(9)$-C_{86} was performed at 173 K on a Bruker D8 QUEST machine equipped with a CMOS camera (Bruker AXS Inc., Germany). Crystallographic characterization of $Lu_2@T_d(2)$-C_{76}, $Lu_2@D_{3h}(5)$-C_{78}, $Lu_2@C_{2v}(5)$-C_{80}, $Lu_2@C_{2v}(7)$-C_{84}, $Lu_2@C_1(26)$-C_{88}, $Lu_2C_2@C_s(32)$-C_{88} and $Lu_2C_2@D_2(35)$-C_{88} was performed at 100 K at BL17B station of the Shanghai Synchrotron Radiation Facility. The multi-scan method was used for absorption corrections. The structures were solved by the direct method and were refined with SHELXL-2014/7.[66] CCDC-1582214 ($Lu_2@T_d(2)$-C_{76}), CCDC-1582215 ($Lu_2@D_{3h}(5)$-C_{78}), CCDC-1582216 ($Lu_2@C_{2v}(5)$-C_{80}), CCDC-1582217 ($Lu_2@C_{2v}(7)$-C_{84}), CCDC-1582218 ($Lu_2@C_s(8)$-C_{86}), CCDC-1582219 ($Lu_2@C_s(15)$-C_{86}), CCDC-1836827 ($Lu_2@C_1(26)$-C_{88}), CCDC-1836828 ($Lu_2C_2@C_{2v}(9)$-C_{86}), CCDC-1836829 ($Lu_2C_2@C_s(32)$-C_{88}) and CCDC-1836830 ($Lu_2C_2@D_2(35)$-C_{88}) contain the supplementary crystallographic data for this paper.†

Computational details

Density functional theory calculations were carried out by using the M06-2X[67] functional in conjunction with the 6-31G* basis set for C[68,69] and SDD basis set and corresponding effective core potential for Lu[70] (denoted as 6-31G*∼SDD), as implemented in the Gaussian 09 software package.[71]

Conflicts of interest

There are no conflicts to declare.

Acknowledgements

The financial support from the NSFC (No. 51472095, 51672093, 51602112, 51602097 and 21103224) is gratefully acknowledged. We thank the staff from BL17B beamline of the National Facility for Protein Science Shanghai (NFPS) at the Shanghai Synchrotron Radiation Facility for assistance during data collection. Also, we are grateful to the Analytical and Testing Center in Huazhong University of Science and Technology for all related measurements.

Notes and references

1 L. Bao, P. Peng and X. Lu, *Acc. Chem. Res.*, 2018, **51**, 810–815.
2 A. A. Popov, S. Yang and L. Dunsch, *Chem. Rev.*, 2013, **113**, 5989–6113.
3 X. Lu, L. Feng, T. Akasaka and S. Nagase, *Chem. Soc. Rev.*, 2012, **41**, 7723–7760.
4 X. Lu, T. Akasaka and S. Nagase, *Acc. Chem. Res.*, 2013, **46**, 1627–1635.
5 T. Cai, L. Xu, M. R. Anderson, Z. Ge, T. Zuo, X. Wang, M. M. Olmstead, A. L. Balch, H. W. Gibson and H. C. Dorn, *J. Am. Chem. Soc.*, 2006, **128**, 8581–8589.
6 S. Stevenson, H. M. Lee, M. M. Olmstead, C. Kozikowski, P. Stevenson and A. L. Balch, *Chem.–Eur. J.*, 2002, **8**, 4528–4535.
7 H. Kurihara, X. Lu, Y. Iiduka, N. Mizorogi, Z. Slanina, T. Tsuchiya, T. Akasaka and S. Nagase, *J. Am. Chem. Soc.*, 2011, **133**, 2382–2385.
8 H. Fang, H. Cong, M. Suzuki, L. Bao, B. Yu, Y. Xie, N. Mizorogi, M. M. Olmstead, A. L. Balch, S. Nagase, T. Akasaka and X. Lu, *J. Am. Chem. Soc.*, 2014, **136**, 10534–10540.
9 T.-S. Wang, N. Chen, J.-F. Xiang, B. Li, J.-Y. Wu, W. Xu, L. Jiang, K. Tan, C.-Y. Shu, X. Lu and C.-R. Wang, *J. Am. Chem. Soc.*, 2009, **131**, 16646–16647.
10 L. Dunsch, S. Yang, L. Zhang, A. Svitova, S. Oswald and A. A. Popov, *J. Am. Chem. Soc.*, 2010, **132**, 5413–5421.
11 N. Chen, M. N. Chaur, C. Moore, J. R. Pinzón, R. Valencia, A. Rodríguez-Fortea, J. M. Poblet and L. Echegoyen, *Chem. Commun.*, 2010, **46**, 4818–4820.
12 Q. Tang, L. Abella, Y. Hao, X. Li, Y. Wan, A. Rodríguez-Fortea, J. M. Poblet, L. Feng and N. Chen, *Inorg. Chem.*, 2015, **54**, 9845–9852.
13 S. Stevenson, M. A. Mackey, M. A. Stuart, J. P. Phillips, M. L. Easterling, C. J. Chancellor, M. M. Olmstead and A. L. Balch, *J. Am. Chem. Soc.*, 2008, **130**, 11844–11845.
14 B. Q. Mercado, M. M. Olmstead, C. M. Beavers, M. L. Easterling, S. Stevenson, M. A. Mackey, C. E. Coumbe, J. D. Phillips, J. Paige Phillips, J. M. Poblet and A. L. Balch, *Chem. Commun.*, 2010, **46**, 279–281.
15 F. Jin, S. Wang, N. B. Tamm, S. Yang and S. I. Troyanov, *Angew. Chem., Int. Ed.*, 2017, **129**, 12152–12156.
16 T.-S. Wang, L. Feng, J.-Y. Wu, W. Xu, J.-F. Xiang, K. Tan, Y.-H. Ma, J.-P. Zheng, L. Jiang, X. Lu, C.-Y. Shu and C.-R. Wang, *J. Am. Chem. Soc.*, 2010, **132**, 16362–16364.
17 F. Liu, C.-L. Gao, Q. Deng, X. Zhu, A. Kostanyan, R. Westerström, S. Wang, Y.-Z. Tan, J. Tao, S.-Y. Xie, A. A. Popov, T. Greber and S. Yang, *J. Am. Chem. Soc.*, 2016, **138**, 14764–14771.
18 X. Zhang, Y. Wang, R. Morales-Martínez, J. Zhong, C. de Graaf, A. Rodríguez-Fortea, J. M. Poblet, L. Echegoyen, L. Feng and N. Chen, *J. Am. Chem. Soc.*, 2018, **140**, 3907–3915.
19 Y. Wang, R. Morales-Martínez, X. Zhang, W. Yang, Y. Wang, A. Rodriguez-Fortea, J. M. Poblet, L. Feng, S. Wang and N. Chen, *J. Am. Chem. Soc.*, 2017, **139**, 5110–5116.
20 W. Cai, R. Morales-Martínez, X. Zhang, D. Najera, E. L. Romero, A. Metta-Magaña, A. Rodríguez-Fortea, S. Fortier, N. Chen, J. M. Poblet and L. Echegoyen, *Chem. Sci.*, 2017, **8**, 5282–5290.
21 A. Rodríguez-Fortea, A. L. Balch and J. M. Poblet, *Chem. Soc. Rev.*, 2011, **40**, 3551–3563.
22 T. Wang and C. Wang, *Acc. Chem. Res.*, 2014, **47**, 450–458.
23 S. Yang, T. Wei and F. Jin, *Chem. Soc. Rev.*, 2017, **46**, 5005–5058.
24 K. Kobayashi and S. Nagase, *Chem. Phys. Lett.*, 1998, **282**, 325–329.
25 L. Bao, C. Pan, Z. Slanina, F. Uhlik, T. Akasaka and X. Lu, *Angew. Chem., Int. Ed.*, 2016, **55**, 9234–9238.
26 S. Yang, S. I. Troyanov, A. A. Popov, M. Krause and L. Dunsch, *J. Am. Chem. Soc.*, 2006, **128**, 16733–16739.

27 M. Krause and L. Dunsch, *ChemPhysChem*, 2004, **5**, 1445–1449.
28 A. A. Popov, M. Krause, S. Yang, J. Wong and L. Dunsch, *J. Phys. Chem. B*, 2007, **111**, 3363–3369.
29 C. M. Beavers, M. N. Chaur, M. M. Olmstead, L. Echegoyen and A. L. Balch, *J. Am. Chem. Soc.*, 2009, **131**, 11519–11524.
30 F. Melin, M. N. Chaur, S. Engmann, B. Elliott, A. Kumbhar, A. J. Athans and L. Echegoyen, *Angew. Chem., Int. Ed.*, 2007, **46**, 9032–9035.
31 M. N. Chaur, F. Melin, J. Ashby, B. Elliott, A. Kumbhar, A. M. Rao and L. Echegoyen, *Chem.–Eur. J.*, 2008, **14**, 8213–8219.
32 A. L. Svitova, A. A. Popov and L. Dunsch, *Inorg. Chem.*, 2013, **52**, 3368–3380.
33 Q. Deng and A. A. Popov, *J. Am. Chem. Soc.*, 2014, **136**, 4257–4264.
34 J. Zhang, T. Fuhrer, W. Fu, J. Ge, D. W. Bearden, J. Dallas, J. Duchamp, K. Walker, H. Champion, H. Azurmendi, K. Harich and H. C. Dorn, *J. Am. Chem. Soc.*, 2012, **134**, 8487–8493.
35 H. Kurihara, X. Lu, Y. Iiduka, H. Nikawa, M. Hachiya, N. Mizorogi, Z. Slanina, T. Tsuchiya, S. Nagase and T. Akasaka, *Inorg. Chem.*, 2012, **51**, 746–750.
36 C.-H. Chen, K. B. Ghiassi, M. R. Cerón, M. A. Guerrero-Ayala, L. Echegoyen, M. M. Olmstead and A. L. Balch, *J. Am. Chem. Soc.*, 2015, **137**, 10116–10119.
37 C.-H. Chen, L. Abella, M. R. Cerón, M. A. Guerrero-Ayala, A. Rodríguez-Fortea, M. M. Olmstead, X. B. Powers, A. L. Balch, J. M. Poblet and L. Echegoyen, *J. Am. Chem. Soc.*, 2016, **138**, 13030–13037.
38 J. Zhang, F. L. Bowles, D. W. Bearden, W. K. Ray, T. Fuhrer, Y. Ye, C. Dixon, K. Harich, R. F. Helm, M. M. Olmstead, A. L. Balch and H. C. Dorn, *Nat. Chem.*, 2013, **5**, 880–885.
39 W. Shen, L. Bao, Y. Wu, C. Pan, S. Zhao, H. Fang, Y. Xie, P. Jin, P. Peng, F.-F. Li and X. Lu, *J. Am. Chem. Soc.*, 2017, **139**, 9979–9984.
40 H. Yang, H. Jin, B. Hong, Z. Liu, C. M. Beavers, H. Zhen, Z. Wang, B. Q. Mercado, M. M. Olmstead and A. L. Balch, *J. Am. Chem. Soc.*, 2011, **133**, 16911–16919.
41 C. M. Beavers, T. Zuo, J. C. Duchamp, K. Harich, H. C. Dorn, M. M. Olmstead and A. L. Balch, *J. Am. Chem. Soc.*, 2006, **128**, 11352–11353.
42 H. Yang, M. Yu, H. Jin, Z. Liu, M. Yao, B. Liu, M. M. Olmstead and A. L. Balch, *J. Am. Chem. Soc.*, 2012, **134**, 5331–5338.
43 T. Zuo, C. M. Beavers, J. C. Duchamp, A. Campbell, H. C. Dorn, M. M. Olmstead and A. L. Balch, *J. Am. Chem. Soc.*, 2007, **129**, 2035–2043.
44 H. Umemoto, K. Ohashi, T. Inoue, N. Fukui, T. Sugai and H. Shinohara, *Chem. Commun.*, 2010, **46**, 5653–5655.
45 Y. Hao, Q. Tang, X. Li, M. Zhang, Y. Wan, L. Feng, N. Chen, Z. Slanina, L. Adamowicz and F. Uhlík, *Inorg. Chem.*, 2016, **55**, 11354–11361.
46 Y.-J. Guo, X. Zhao, P. Zhao and T. Yang, *J. Phys. Chem. A*, 2015, **119**, 10428–10439.
47 W. Cai, L. Bao, S. Zhao, Y. Xie, T. Akasaka and X. Lu, *J. Am. Chem. Soc.*, 2015, **137**, 10292–10296.
48 W. Cai, F.-F. Li, L. Bao, Y. Xie and X. Lu, *J. Am. Chem. Soc.*, 2016, **138**, 6670–6675.
49 S. Zhao, P. Zhao, W. Cai, L. Bao, M. Chen, Y. Xie, X. Zhao and X. Lu, *J. Am. Chem. Soc.*, 2017, **139**, 4724–4728.
50 T. Yang, X. Zhao and E. Osawa, *Chem.–Eur. J.*, 2011, **17**, 10230–10234.
51 J. Hao, F. Li, H. Li, X. Chen, Y. Zhang, Z. Chen and C. Hao, *RSC Adv.*, 2015, **5**, 34383–34389.
52 B. Christen, H. Christen and S. Xin, *J. Am. Chem. Soc.*, 2017, **139**, 3919.
53 X. Lu, Z. Slanina, T. Akasaka, T. Tsuchiya, N. Mizorogi and S. Nagase, *J. Am. Chem. Soc.*, 2010, **132**, 5896–5905.
54 A. A. Popov, S. M. Avdoshenko, A. M. Pendás and L. Dunsch, *Chem. Commun.*, 2012, **48**, 8031.
55 N. A. Samoylova, S. M. Avdoshenko, D. S. Krylov, H. R. Thompson, A. C. Kirkhorn, M. Rosenkranz, S. Schiemenz, F. Ziegs, A. U. B. Wolter, S. Yang, S. Stevenson and A. A. Popov, *Nanoscale*, 2017, **23**, 7977–7990.
56 A. Velloth, Y. Imamura, T. Kodama and M. Hada, *J. Phys. Chem. C*, 2017, **121**, 18169–18177.
57 Z. Wang, R. Kitaura and H. Shinohara, *J. Phys. Chem. C*, 2014, **118**, 13953–13958.
58 Y. Maeda, T. Tsuchiya, T. Kikuchi, H. Nikawa, T. Yang, X. Zhao, Z. Slanina, M. Suzuki, M. Yamada, Y. Lian, S. Nagase, X. Lu and T. Akasaka, *Carbon*, 2016, **98**, 67–73.
59 H. Yang, C. Lu, Z. Liu, H. Jin, Y. Che, M. M. Olmstead and A. L. Balch, *J. Am. Chem. Soc.*, 2008, **130**, 17296–17300.
60 A. L. Balch, M. M. Olmstead, X. Powers, C. M. Davison, S. Stevenson and K. R. Tepper, *Chem.–Eur. J.*, 2018, **24**, 13479–13484.
61 M. Yamada, Y. Muto, H. Kurihara, Z. Slanina, M. Suzuki, Y. Maeda, Y. Rubin, M. M. Olmstead, A. L. Balch, S. Nagase, X. Lu and T. Akasaka, *Angew. Chem., Int. Ed.*, 2015, **54**, 2232–2235.
62 M. Suzuki, N. Mizorogi, T. Yang, F. Uhlik, Z. Slanina, X. Zhao, M. Yamada, Y. Maeda, T. Hasegawa, S. Nagase, X. Lu and T. Akasaka, *Chem.–Eur. J.*, 2013, **19**, 17125–17130.
63 B. Cao, H. Nikawa, T. Nakahodo, T. Tsuchiya, Y. Maeda, T. Akasaka, H. Sawa, Z. Slanina, N. Mizorogi and S. Nagase, *J. Am. Chem. Soc.*, 2008, **130**, 983–989.
64 L. Bao, M. Chen, C. Pan, T. Yamaguchi, T. Kato, M. M. Olmstead, A. L. Balch, T. Akasaka and X. Lu, *Angew. Chem., Int. Ed.*, 2016, **55**, 4242–4246.
65 C. M. Beavers, H. Jin, H. Yang, Z. Wang, X. Wang, H. Ge, Z. Liu, B. Q. Mercado, M. M. Olmstead and A. L. Balch, *J. Am. Chem. Soc.*, 2011, **133**, 15338–15341.
66 G. M. Sheldrick, *Acta Crystallogr., Sect. A: Found. Crystallogr.*, 2008, **64**, 112–122.
67 Y. Zhao and D. G. Truhlar, *Theor. Chem. Acc.*, 2008, **120**, 215–241.
68 G. A. Petersson and M. A. Al-Laham, *J. Chem. Phys.*, 1991, **94**, 6081–6090.
69 G. A. Petersson, A. Bennett, T. G. Tensfeldt, M. A. Al-Laham, W. A. Shirley and J. Mantzaris, *J. Chem. Phys.*, 1988, **89**, 2193–2218.
70 X. Cao and M. Dolg, *J. Mol. Struct.: THEOCHEM*, 2002, **581**, 139–147.
71 M. J. Frisch, G. W. Trucks, H. B. Schlegel, G. E. Scuseria, M. A. Robb, J. R. Cheeseman, G. Scalmani, V. Barone, B. Mennucci, G. A. Petersson, *et al.*, *Gaussian 09*, Gaussian, Inc., Wallingford, CT, USA, 2009.